LETTER

https://doi.org/10.1038/s41586-018-0589-x

# Glacial expansion of oxygen-depleted seawater in the eastern tropical Pacific

Babette A. A. Hoogakker[1,2]*, Zunli Lu[3,4]*, Natalie Umling[5], Luke Jones[2], Xiaoli Zhou[6], Rosalind E. M. Rickaby[2], Robert Thunell[5,10], Olivier Cartapanis[7] & Eric Galbraith[8,9]

**Increased storage of carbon in the oceans has been proposed as a mechanism to explain lower concentrations of atmospheric carbon dioxide during ice ages; however, unequivocal signatures of this storage have not been found[1]. In seawater, the dissolved gases oxygen and carbon dioxide are linked via the production and decay of organic material, with reconstructions of low oxygen concentrations in the past indicating an increase in biologically mediated carbon storage. Marine sediment proxy records have suggested that oxygen concentrations in the deep ocean were indeed lower during the last ice age, but that near-surface and intermediate waters of the Pacific Ocean—a large fraction of which are poorly oxygenated at present—were generally better oxygenated during the glacial[1–3]. This vertical opposition could suggest a minimal net basin-integrated change in carbon storage. Here we apply a dual-proxy approach, incorporating qualitative upper-water-column and quantitative bottom-water oxygen reconstructions[4,5], to constrain changes in the vertical extent of low-oxygen waters in the eastern tropical Pacific since the last ice age. Our tandem proxy reconstructions provide evidence of a downward expansion of oxygen depletion in the eastern Pacific during the last glacial, with no indication of greater oxygenation in the upper reaches of the water column. We extrapolate our quantitative deep-water oxygen reconstructions to show that the respired carbon reservoir of the glacial Pacific was substantially increased, establishing it as an important component of the coupled mechanism that led to low levels of atmospheric carbon dioxide during the glacial.**

The modern-day Pacific Ocean contains a vast volume of oxygen-depleted waters. In the eastern basin north of 18° S, waters deeper than 1 km (deepening to 2 km north of the Equator) are generally oxic (with an oxygen concentration, $[O_2]$, of more than 120 μmol $kg^{-1}$), whereas at shallower depths most waters are hypoxic ($[O_2] < 60–120$ μmol $kg^{-1}$), and a small fraction are suboxic[6] ($[O_2] < 2–10$ μmol $kg^{-1}$). The eastern tropical North Pacific (ETNP) oxygen minimum zone (OMZ) is the world's largest OMZ, and currently encompasses 67% of the suboxic waters on Earth[6]. Low-oxygen conditions place important limitations on marine life, with hypoxic conditions proving lethal for more than half of marine benthic animal species[7]. Oceanic nutrient cycling is also affected by suboxic conditions[8,9], under which the remineralization of organic material occurs via anaerobic metabolic pathways, including denitrification and anammox. This removes bioavailable nitrogen (which supports primary production) from the ocean and generates the greenhouse gas nitrous oxide.

Because of the intrinsic link between oxygen and carbon in photosynthesis and respiration, oxygen utilization provides a direct reflection of the strength of the biological carbon pump and therefore its influence on atmospheric $CO_2$[4]. Today, the Pacific Ocean represents the largest modern sink of respired organic carbon (>730 Gt, around 50% of the global ocean inventory[10]), half of which resides in the upper 1.5 km.

The concentration of dissolved oxygen in seawater is controlled by two factors: first, the saturation oxygen concentration of seawater in contact with the atmosphere, which is the sum of oxygen solubility (a function of temperature and salinity) and any disequilibrium from saturation at the ocean surface; and second, the net oxygen utilization, which is determined by the accumulated consumption during remineralization of organic material along the pathways of advection and mixing[8]. Over the past 50 years the observed vertical expansion of the equatorial Pacific OMZ has been attributed mostly to a net increase in oxygen utilization, which could reflect a reduced input rate of oxygen through advection and mixing and/or an increase in the local rate of respiration by organic matter[11,12]. A further decline in ocean oxygen levels is predicted by Earth system models under anthropogenic warming, linked to increased temperatures (lowering the saturation oxygen concentration) and increased oxygen utilization owing to decreased ventilation[8,11,13]. However, model simulations disagree about oxygen changes in the tropical thermoclines, and do not reproduce the large historical changes[11], which suggests that these models are missing important processes that may compromise their predictions of future change[13,14].

Reconstructions of the last ice age offer an alternative test of the link between climate and ocean oxygenation. Lower glacial seawater temperatures would have increased oxygen saturation concentrations[2] and decreased remineralization rates[15]. These conditions could have resulted in a better-oxygenated upper ocean, potentially eliminating the OMZs. Bulk sedimentary nitrogen isotope ($\delta^{15}N$) records from the eastern tropical Pacific (ETP)[16,17] have been interpreted to reflect overall reduced glacial denitrification rates in the upper water column[18], which could indicate an absence of suboxic waters. By contrast, the cold-enhanced solubility appears to have been overwhelmed by increased oxygen utilization in the deep Pacific, resulting in reduced oxygen concentrations and increased respired carbon storage that could have contributed to the low atmospheric $CO_2$ concentrations[1–3]. However, these reconstructions are based on qualitative proxies, which are often difficult to interpret[19]. Furthermore, many of these records have been limited to core sites from continental slopes, and are potentially biased by local conditions[19].

To constrain upper-water-column oxygen concentrations, we used planktonic foraminifera I/Ca ratios[5] (see Methods). This proxy takes advantage of iodine speciation in seawater. The iodate species ($IO_3^-$) is favoured under well-oxygenated settings, whereas iodide ($I^-$) becomes the dominant species under oxygen-depleted conditions. Because foraminiferal calcite incorporates only iodate, the foraminiferal I/Ca ratio therefore reflects the abundance of the oxidised form[20].

Furthermore, we use the benthic foraminiferal carbon-isotope gradient proxy ($\Delta\delta^{13}C$) to quantitatively reconstruct bottom-water oxygen concentrations[4]. The $\Delta\delta^{13}C$ between bottom water and pore water at the anoxic boundary in sediments is related to the oxygen concentration of the overlying bottom waters[21]. The $\Delta\delta^{13}C$ between

[1]The Lyell Centre, Heriot-Watt University, Edinburgh, UK. [2]Department of Earth Sciences, University of Oxford, Oxford, UK. [3]Department of Earth Sciences, Syracuse University, Syracuse, NY, USA. [4]State Key Laboratory of Marine Environmental Science, Xiamen University, Xiamen, China. [5]School of Earth, Ocean and Environment, University of South Carolina, Columbia, SC, USA. [6]Department of Marine and Coastal Sciences, Rutgers University, New Brunswick, NJ, USA. [7]University of Bern, Oeschger Centre for Climate Change Research, Bern, Switzerland. [8]Institut de Ciencia i Tecnologia Ambientals (ICTA) and Department of Mathematics, Universitat Autonoma de Barcelona, Bellaterra, Spain. [9]ICREA, Barcelona, Spain. [10]Deceased: Robert Thunell. *e-mail: b.hoogakker@hw.ac.uk; zunlilu@syr.edu

bottom water and pore water at the anoxic boundary is reproduced by the $\Delta\delta^{13}C$ of benthic foraminifera with microhabitats in bottom water (*Cibicidoides wuellerstorfi*) and in sediments at the anoxic boundary (*Globobulimina* spp.)[4]. This method enables us to quantitatively reconstruct past dissolved oxygen concentrations in the range of 55–235 μmol $kg^{-1}$ (see Methods) in bottom waters from tropical to temperate regions, with an estimated total standard error[4] of 17 μmol $kg^{-1}$. Our tandem proxy approach enables us to place firm constraints on past changes in the geometry of oxygen-depleted waters in the eastern tropical Pacific over the past 40,000 years. Furthermore, extrapolation of our new quantitative bottom-water oxygen reconstructions enables us to calculate the change in size of the Pacific respired-carbon pool and assess its role in glacial–interglacial $CO_2$ cycles.

Planktonic foraminifera I/Ca ratios were measured at two eastern tropical Pacific sites. ODP site 1242 (7.86° N, 83.61° W, 1.36 km) is on the Costa Rica margin, in the eastern tropical North Pacific (ETNP), whereas ODP site 849 (0.18° N, 110.50° W, 3.85 km) lies beneath the eastern equatorial cold tongue (Fig. 1). Planktonic foraminifera I/Ca ratios at the ETNP site are expected to monitor changes in the upper boundary of the ETNP-OMZ. The cold tongue site, ODP site 849, is distal from modern suboxic zones but downstream of waters that have passed through them, and planktonic foraminifera I/Ca ratios at this location are expected to have responded to the broader presence of oxygen-depleted waters within the ETP-OMZ. The location of ODP site 1242 at the deep boundary of the present-day ETNP-OMZ is ideal to test for changes in the vertical extent of the OMZ, via benthic foraminifera $\Delta\delta^{13}C$. Additionally, bottom-water oxygen concentrations were reconstructed for deep water at TR163-25 (1.65° S, 88.45° W, 2.65 km), to provide quantitative estimates of changes in deep-water oxygen concentrations in the eastern tropical Pacific and calculate the glacial increase in the deep Pacific respired-carbon pool. Details of age models are provided in Extended Data Tables 1, 2 and Extended Data Fig. 1.

Modern oxygen profiles at ODP sites 849 and 1242 are very similar (Fig. 1), except that OMZ waters ($[O_2]$ threshold[22] < 45 μmol $kg^{-1}$) occur at a much shallower depth at the ETNP site (within the upper 50 m) compared to the cold tongue site (deeper than 250 m) (Fig. 1). This difference in the upper water column is consistent with the contrasting core–top planktonic foraminifera I/Ca values at the two sites (Fig. 2). If suboxia had been reduced during the glacial, as has been previously suggested, one would expect high I/Ca values to be found in glacial-age foraminifera. Instead we find that low I/Ca values (<0.6 μmol $mol^{-1}$) prevailed continuously over the past 40 thousand years (kyr) at the ETNP-OMZ site, which is consistent with persistent oxygen depletion at shallow depths (Fig. 2). Furthermore, although I/Ca ratios of all planktonic species in the cold tongue from 40–25 kyr before present (BP) were similar to values from the late Holocene, during early deglaciation (around 18–16 kyr BP) the I/Ca of shallow-dwelling species decreased to values as low as those of the thermocline species. The persistently depleted planktonic foraminifera oxygen isotope values of the shallow-dwelling species and the heavy values of the thermocline species (Fig. 2) indicate similar depth habitats over the past 40 kyr. Therefore, we attribute the lower I/Ca values of the shallow-dwelling species at site 849 during early deglaciation to the increased presence of oxygen-depleted waters in the ETP-OMZ.

Turning to the deep sea, reconstructed dissolved oxygen at ODP site 1242 shows generally lower concentrations during the glacial compared to the Holocene, with an average Last Glacial Maximum (LGM) (18–22 kyr BP) dissolved oxygen content of 55 μmol $kg^{-1}$ (±17 μmol $kg^{-1}$, Fig. 3). The lowest oxygen concentrations (44 μmol $kg^{-1}$) were recorded during early deglaciation (17–15 kyr BP), followed by a rapid increase in the mid- to late deglaciation. Maximum oxygen concentrations of 100 μmol $kg^{-1}$ were recorded during the early Holocene. Oxygenation then decreased slightly through the Holocene, reaching late Holocene values of 85 μmol $kg^{-1}$ (Fig. 3). At the deeper site TR163-25, reconstructed LGM oxygen concentrations are similar to those of ODP site 1242, averaging 54 μmol $kg^{-1}$ (Fig. 3), and there is also a brief decline in dissolved oxygen during the early deglaciation to around

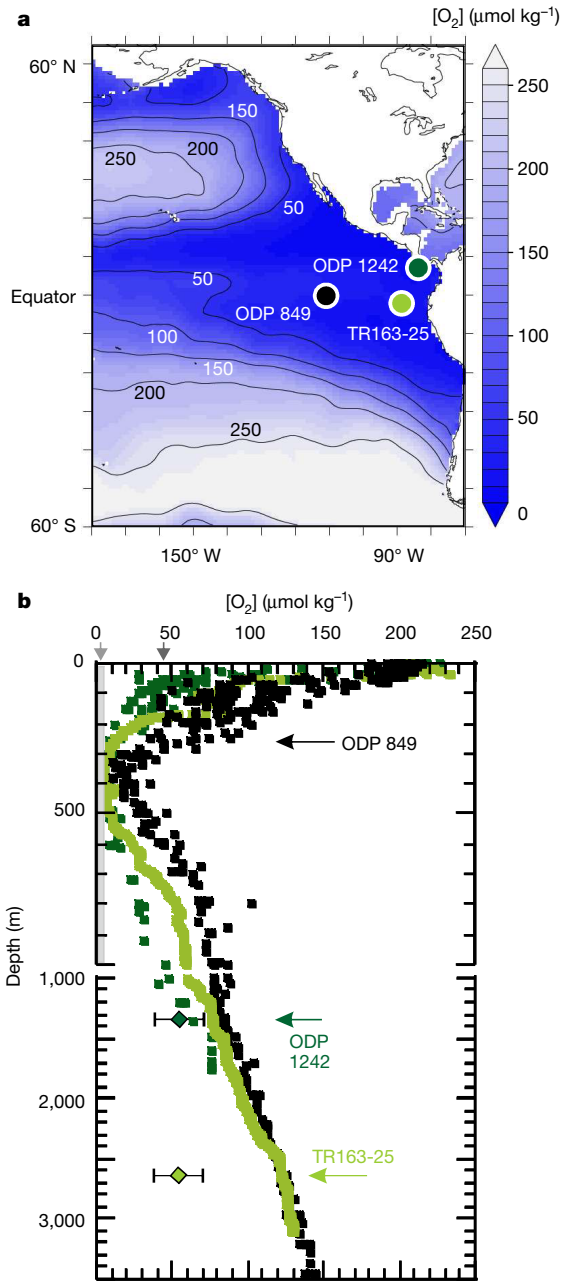


**Fig. 1 | Overview of dissolved oxygen concentrations in the eastern Pacific Ocean. a**, Oxygen concentrations between 60° S and 60° N at 400 m water depth (circles show core locations). Data are from ref. [28]. **b**, Vertical profiles at the core sites (from https://www.nodc.noaa.gov/OC5/SELECT/dbsearch/dbsearch.html; data from ref. [28]). ODP site 1242, dark green; ODP site 849, black; TR163-25, light green. Note the different scales for the upper part (0–1,000 m) and the lower part (1,000–4,000 m) of the water column. Arrows on the *x* axis indicate $[O_2]$ thresholds for suboxia (light grey) and the OMZ (dark grey). Diamonds illustrate the reconstructed LGM bottom-water $[O_2]$ values at ODP site 1242 and TR163-25, including ±17 μmol $kg^{-1}$ error[4].

40 μmol $kg^{-1}$, followed by a rapid increase to around 160 μmol $kg^{-1}$ in the mid-Holocene (Fig. 3).

Our dual-proxy results from the upper 1.4 km of the water column (planktonic foraminifera I/Ca at ODP sites 1242 and 849, $\Delta\delta^{13}C$ at ODP site 1242) show sustained oxygen depletion; this is in contrast with other studies, which have suggested that the upper water column in the Pacific was generally more oxygenated at this time[1–3]. These previous conclusions were based on observations of low sedimentary $\delta^{15}N$ (interpreted as lower rates of denitrification), weaker sedimentary

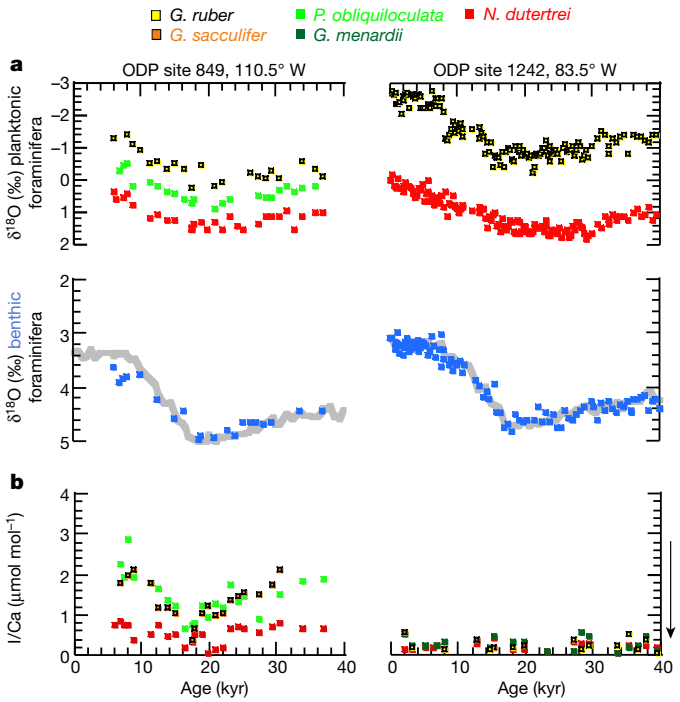


**Fig. 2 | Reconstructed ETP surface water oxygenation. a**, Planktonic foraminiferal and benthic composite oxygen isotope ($\delta^{18}O$) records (blue symbols) and stacked records (grey lines)[29] at ODP sites 849 and 1242. Planktonic foraminiferal oxygen isotopes at ODP site 1242 until 28 kyr BP are from ref. [30]. Details of age models can be found in Methods. **b**, I/Ca ratios of planktonic foraminifera. I/Ca ratios of less than 2.5 μmol $mol^{-1}$ are indicative of the presence of low-oxygen waters in the upper 400 m of the water column[5]. The arrow indicates the increasing influence of oxygen depletion.

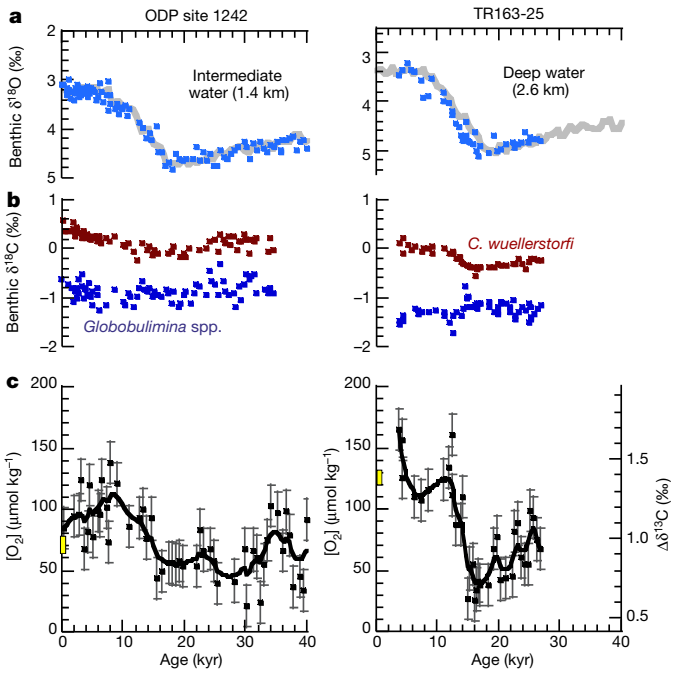


**Fig. 3 | Reconstructed ETP bottom-water oxygen concentrations.** **a**, Benthic foraminiferal $\delta^{18}O$ (blue symbols) of ODP site 1242 and TR163-25 (*C. wuellerstorfi*, adjusted by +0.64‰) and stacked records (grey lines) from the intermediate and deep Pacific[29]. Details of age models can be found in Methods. **b**, Benthic foraminiferal carbon isotopes of *C. wuellerstorfi* (red) and *Globobulimina* spp. (blue). **c**, Reconstructed bottom-water $[O_2]$ and $\Delta\delta^{13}C$ (raw data[4], black squares + total error of ±17 μmol $kg^{-1}$; thick line shows moving average calculated using the boxcar algorithm). Yellow boxes indicate the modern range of bottom-water oxygen concentrations.

laminations and lower abundances of oxygen-sensitive trace metals during the glacial[2]. However, there are several reasons that sedimentary $\delta^{15}N$ could have been lower during the glacial without a substantial change in oxygen concentrations (see Methods and Extended Data Fig. 2). Furthermore, the sedimentary laminations and trace metals previously examined at three sites in the coastal ETP showed only weak signs of oxygen change between the LGM and the Holocene[16,17], which could also be attributed to changes in the characteristics of accumulating sediments[23,24]. Therefore, the persistently low I/Ca values, in combination with reduced glacial bottom-water oxygen levels at 1.4 km (today the lower boundary of the ETNP-OMZ), do not support a substantial contraction of the upper reaches of the tropical Pacific OMZ during the glacial period compared to today.

Our results also indicate a period of particularly strong oxygen depletion during the early deglaciation, which is consistent with previous sedimentary $\delta^{15}N$ values, lamination, and trace metal evidence from the ETNP[16,17]. The convergence of mixed-layer and thermocline planktonic foraminifera to low values of I/Ca at ODP site 849 (Fig. 2) suggests that the downward expansion of oxygen-depleted waters in the ETP-OMZ, indicated by the bottom-water oxygen reconstructions (Fig. 3), was accompanied by an intensified influence of oxygen depleted-waters in the upper water column. The interval coincides with a weak Atlantic Meridional Overturning Circulation, and an apparent productivity peak in the eastern equatorial Pacific that is speculated to reflect an increased delivery of nutrients from southern-sourced deep waters and intensified upwelling[17,25–27].

Our tandem proxy results provide new insights into the evolution of respired carbon storage in the eastern tropical Pacific since the last ice age. Today, a quarter of the total global respired carbon reservoir is stored in the upper 1.5 km (intermediate and subsurface waters) of the Pacific. Our results suggest that the respired-carbon reservoir of the upper water column has shown little change between the LGM and the Holocene, whereas that of the deeper Pacific has increased, suggesting a net increase in the size of the Pacific glacial respired-carbon pool.

Furthermore, the results of $\Delta\delta^{13}C$ analysis show that the modern vertical-oxygen gradient ($\Delta[O_2]$, of around 65 μmol $kg^{-1}$) between water depths of 1.4 km and 2.6 km was eliminated during the LGM (Fig. 1), so that oxygen concentrations did not increase with depth as they do today. We also find that the gradient of $\delta^{13}C$ in the dissolved inorganic carbon between these water masses was reversed (Extended Data Fig. 3), as would be expected given the respired carbon concentrations inferred from our quantitative oxygen reconstructions and similar changes in the preformed component of $\delta^{13}C$ (for details, see Methods). Our data therefore suggest that, despite large changes in the average $\delta^{13}C$ of dissolved inorganic carbon for the whole ocean and changes in air–sea exchange, the relative change in $\delta^{13}C$ between sites in the depth range of 1.4 km to 3 km provides a good approximation of the change in oxygen concentrations.

We take advantage of this new constraint, together with our LGM–modern $\delta^{13}C$ compilation, to extrapolate our results spatially in the deep Pacific. Our results suggest that the total amount of respired carbon in the Pacific was approximately 90 Gt greater between water depths of 1.4 km and 3 km, and possibly 200 Gt greater across the whole of the deep Pacific (see Methods), during the LGM compared with today. This provides a useful new target for model simulations of glacial carbon cycling. Although the average increase in respired carbon concentrations in deeper waters of the Pacific is only half that of the deep Atlantic[4], the estimated glacial increase in its respired carbon reservoir is almost three times that of the deep Atlantic owing to its vast size. This suggests that the Pacific made an important contribution to glacial–interglacial changes in atmospheric $CO_2$ levels.

## Online content

Any methods, additional references, Nature Research reporting summaries, source data, statements of data availability and associated accession codes are available at https://doi.org/10.1038/s41586-018-0589-x.

Received: 3 July 2017; Accepted: 13 August 2018;
Published online 17 October 2018.

1. Sigman, D. M. & Boyle, E. A. Glacial/interglacial variations in atmospheric carbon dioxide. *Nature* **407**, 859–869 (2000).
2. Galbraith, E. D. & Jaccard, S. L. Deglacial weakening of the oceanic soft tissue pump: global constraints from sedimentary nitrogen isotopes and oxygenation proxies. *Quat. Sci. Rev.* **109**, 38–48 (2015).
3. Bradtmiller, L. I., Anderson, R. F., Sachs, J. P. & Fleisher, M. Q. A deeper respired carbon pool in the glacial equatorial Pacific Ocean. *Earth Planet. Sci. Lett.* **299**, 417–425 (2010).
4. Hoogakker, B. A. A., Elderfield, H., Schmiedl, G., McCave, I. N. & Rickaby, R. E. M. Glacial–interglacial changes in bottom-water oxygen content on the Portuguese margin. *Nat. Geosci.* **8**, 40–43 (2015).
5. Lu, Z. et al. Oxygen depletion recorded in upper waters of the glacial Southern Ocean. *Nat. Commun.* **7**, 11146 (2016).
6. Bianchi, D., Dunne, J. P., Sarmiento, J. L. & Galbraith, E. D. Data-based estimates of suboxia, denitrification, and $N_2O$ production in the ocean and their sensitivities to dissolved $O_2$. *Global Biogeochem. Cycles* **26**, (2012).
7. Vaquer-Sunyer, R. & Duarte, C. M. Thresholds of hypoxia for marine biodiversity. *Proc. Natl Acad. Sci. USA* **105**, 15452–15457 (2008).
8. Keeling, R. E., Körtzinger, A. & Gruber, N. Ocean deoxygenation in a warming world. *Ann. Rev. Mar. Sci.* **2**, 199–229 (2010).
9. Lam, P. & Kuypers, M. M. M. Microbial nitrogen cycling processes in oxygen minimum zones. *Ann. Rev. Mar. Sci.* **3**, 317–345 (2011).
10. Schmittner, A. & Somes, C. J. Complementary constraints from carbon ($^{13}C$) and nitrogen ($^{15}N$) isotopes on the glacial ocean's soft-tissue biological pump. *Paleoceanography* **31**, 669–693 (2016).
11. Schmidtko, S., Stramma, L. & Visbeck, M. Decline in global oceanic oxygen content during the past five decades. *Nature* **542**, 335–339 (2017).
12. Stramma, L., Johnson, G. C., Sprintall, J. & Mohrholz, V. Expanding oxygen-minimum zones in the tropical oceans. *Science* **320**, 655–658 (2008).
13. Bopp, L. et al. Multiple stressors of ocean ecosystems in the 21st century: projections with CMIP5 models. *Biogeosciences* **10**, 6225–6245 (2013).
14. Long, M., Deutsch, C. & Ito, I. Finding forced trends in oceanic oxygen. *Global Biogeochem. Cycles* **30**, 381–397 (2016).
15. Matsumoto, K. Biology-mediated temperature control on atmospheric $pCO_2$ and ocean biogeochemistry. *Geophys. Res. Lett.* **34**, L20605 (2007).
16. Pichevin, L. E. et al. Interhemispheric leakage of isotopically heavy nitrate in the eastern tropical Pacific during the last glacial period. *Paleoceanography* **25**, PA1204 (2010).
17. Hendy, I. L. & Pedersen, T. F. Oxygen minimum zone expansion in the eastern tropical North Pacific during deglaciation. *Geophys. Res. Lett.* **33**, L20602 (2006).
18. Galbraith, E. D., Kienast, M. & The NICOPP working group members. The acceleration of ocean denitrification during deglacial warming. *Nat. Geosci.* **6**, 579–584 (2013).
19. Moffitt, S. E. et al. Paleoceanographic insights on recent oxygen minimum zone expansion: lessons for modern oceanography. *PLoS ONE* **10**, e0115246 (2015).
20. Lu, Z., Jenkyns, H. C. & Rickaby, R. E. M. Iodine to calcium ratios in marine carbonates as a paleo-redox proxy during oceanic anoxic events. *Geology* **38**, 1107–1110 (2010).
21. McCorkle, D. C. & Emerson, S. R. The relationship between pore water carbon isotopic composition and bottom water oxygen concentration. *Geochim. Cosmochim. Acta* **52**, 1169–1178 (1988).
22. Karstensen, J., Stramma, L. & Visbeck, M. Oxygen minimum zones in the eastern tropical Atlantic and Pacific oceans. *Prog. Oceanogr.* **77**, 331–350 (2008).
23. van Geen, A. et al. On the preservation of laminated sediments along the western margin of North America. *Paleoceanography* **18**, 1098 (2003).
24. Nameroff, T. J., Calvert, E. & Murray, J. W. Glacial–interglacial variability in the eastern tropical North Pacific oxygen minimum zone recorded by redox-sensitive trace metals. *Paleoceanography* **19**, PA1010 (2004).
25. Costa, K. M. et al. Productivity patterns in the Equatorial Pacific over the last 30,000 years. *Global Biogeochem. Cycles* **31**, 850–865 (2017).
26. Kienast, M. et al. Eastern Pacific cooling and Atlantic overturning circulation during the last deglaciation. *Nature* **443**, 846–849 (2006).
27. de la Fuente, M., Skinner, L., Calvo, E., Pelejero, C. & Cacho, I. Increased reservoir ages and poorly ventilated deep waters inferred in the glacial Eastern Equatorial Pacific. *Nat. Commun.* **6**, 7420 (2015).
28. Garcia, H. et al. *World Ocean Atlas 2013, Volume 3: Dissolved Oxygen, Apparent Oxygen Utilization, and Oxygen Saturation* (ed. Levitus, S.) (NOAA Atlas NESDIS 75, 2013).
29. Stern, J. V. & Lisiecki, L. E. Termination 1 timing in radiocarbon-dated regional benthic $\delta^{18}O$ stacks. *Paleoceanography* **29**, 1127–1142 (2014).
30. Benway, H. M., Mix, A. C., Haley, B. A. & Klinkhammer, G. P. Eastern Pacific warm pool paleosalinity and climate variability: 0–30 kyr. *Paleoceanography* **21**, PA3008 (2006).

**Acknowledgements** This study benefited from discussions with R. Ganeshram. This work is supported by UK Natural Environment Research Council (NERC) grant NE/I020563/1 (to B.A.A.H.), National Science Foundation (NSF) grants OCE-1232620 and OCE-1736542 (to Z.L.) and Swiss National fund PP00P2_144811 (to O.C.). This research used samples and/or data provided by the Ocean Drilling Program (ODP). ODP is sponsored by the US National Science Foundation and participating countries (Natural Environment Research Council in the UK) under the management of Joint Oceanographic Institutions (JOI), Inc. M. Hall, J. Rolfe and C. Day are acknowledged for help with stable isotope analyses.

**Author contributions** B.A.A.H. and Z.L. conceived and coordinated the work. B.A.A.H., Z.L., N.U., L.J. and X.Z. carried out data analyses; O.C. carried out data synthesis. B.A.A.H., Z.L. and E.G. constructed the figures and wrote the paper, with contributions from the other co-authors.

**Competing interests** The authors declare no competing interests.

**Additional information**
**Extended data** is available for this paper at https://doi.org/10.1038/s41586-018-0589-x.
**Reprints and permissions information** is available at http://www.nature.com/reprints.
**Correspondence and requests for materials** should be addressed to B.A.A.H. or Z.L.
**Publisher's note:** Springer Nature remains neutral with regard to jurisdictional claims in published maps and institutional affiliations.

## METHODS

**Analytical methods.** Foraminifera oxygen and carbon isotopes for ODP sites 849 and 1242 were measured using a Thermo MAT253 IRMS coupled to a Kiel Device at the Godwin Laboratory (University of Cambridge) and a Thermo Delta V Advantage coupled to a Kiel Device at the Department of Earth Sciences (University of Oxford). Calibration to Vienna Pee Dee Belemnite was via NBS19 standards. Overall precision for $\delta^{18}O$ is $\sigma = 0.07‰$ (Oxford) and $\sigma = 0.08‰$ (Cambridge), and for $\delta^{13}C$ is $\sigma = 0.04‰$ (Oxford) and $\sigma = 0.06‰$ (Cambridge). For benthic foraminifera analyses we typically used 3–5 specimens of *C. wuellerstorfi*, 6 specimens of *C. pachyderma*, and >4 specimens of *Globobulimina* spp. For planktonic foraminifera analyses a minimum of 20 specimens were analysed. For site TR163-25 benthic foraminifera, oxygen and carbon isotopes, as well as (homogenized) bulk sedimentary nitrogen isotopes, were measured on a GV Isoprime stable isotope ratio mass spectrometer at the University of South Carolina, with a long-term laboratory reproducibility of 0.07‰ (oxygen) 0.06‰ (carbon), and 0.14‰ (nitrogen). Typically 1–5 *Globobulimina* spp. and *C. wuellerstorfi* were used for benthic foraminifera stable isotope analyses at site TR163-25.

Planktonic foraminifera I/Ca ratios were measured by quadrupole ICP-MS (Bruker M90) at Syracuse University, using a previously published method[5]. The sensitivity of iodine was tuned to above 80 kcps for a 1 p.p.b. standard. Iodine calibration standards were freshly prepared from $KIO_3$ powder. The precision for $^{127}I$ is typically better than 1%. The detection limit of I/Ca is on the order of 0.1 μmol $mol^{-1}$.

**Age models.** The age models for ODP sites 849 and 1242 are based on oxygen-isotope stratigraphy, matching new benthic foraminiferal $\delta^{18}O$ records (Extended Data Fig. 1, Extended Data Table 1) to the Pacific intermediate and deep-stacked $\delta^{18}O$ records of ref. [29]. The benthic composite $\delta^{18}O$ record of ODP site 849 features specimens of *C. wuellerstorfi*, *Laticarinina pauperata* (both adjusted by +0.64‰ to bring them closer to values of *Uvigerina* spp.), and *Uvigerina* spp. The composite record of ODP site 1242 $\delta^{18}O$ includes mainly specimens of *C. wuellerstorfi*, *Cibicidoides pachyderma* (both adjusted by +0.64‰), and minor contributions from *Uvigerina peregrina*.

For TR163-25 the chronology was developed using one *G. ruber* and three *N. dutertrei* $^{14}C$ ages (Extended Data Table 2) calibrated with reservoir ages calculated for the EEP from TR163-23[31] and ODP site 1240[27] using the Bayesian age model program BACON[32].

**Bottom-water oxygen concentrations.** It has been shown[4] that there is a strong ($R^2 = 0.94$) linear relationship between bottom-water oxygen concentrations and $\Delta\delta^{13}C$ at oxygen levels between 55 and 235 μmol $kg^{-1}$, with an approximately 0.4‰ increase in $\Delta\delta^{13}C$ for every 50 μmol $kg^{-1}$ increase in bottom-water oxygen concentrations. According to ref. [4], the total error associated with bottom-water oxygen concentration at mid- to low latitudes is ±17 μmol $kg^{-1}$. When oxygen concentrations exceed 255 μmol $kg^{-1}$, the relationship with $\Delta\delta^{13}C$ weakens owing to $\delta^{13}C$ of *Globobulimina* spp. becoming much more depleted. This typically occurs in environments in which the oxygen penetration depth is greater than the depth of the sediment mixed layer causing the addition of light carbon through sulfate reduction[21]. At oxygen concentrations between 50 and 20 μmol $kg^{-1}$ we expect the strong linear relationship ($\Delta\delta^{13}C = 0.00772 \times$ (dissolved oxygen concentration) + 0.41446) to hold, as aerobic respiration still dominates the remineralization of organic carbon[33]. This is supported by two new data points derived from temperate North Pacific Holocene samples of ODP sites 1014 ($[O_2] = 32 \pm 10$ μmol $kg^{-1}$; $\Delta\delta^{13}C = 0.54‰ \pm 0.03‰$) and 1019 ($[O_2] = 21 \pm 6$ μmol $kg^{-1}$; $\Delta\delta^{13}C = 0.44‰ \pm 0.1‰$). At ODP site 1242, one data point from around 38 kyr BP fell outside of the calibration (reconstructed $[O_2]$ of 16 μmol $kg^{-1}$) and is not shown in Fig. 3. At ODP site 1242, products of manganese and iron reduction ($Mn^{2+}$ and $Fe^{2+}$) become important below 50 m composite depth[34] (reconstructions of $\Delta\delta^{13}C$ only took place between 0 and 6.5 m). Therefore, we do not expect deviations in $\Delta\delta^{13}C$ in relation to these processes. The most recent Holocene is missing from core 1242, as evidenced by high core top $\delta^{13}C$ of *C. wuellerstorfi* (average 0.4‰ top 25 cm) in contrast with seawater $\delta^{13}C$ of dissolved inorganic carbon (DIC) of −0.2‰ to −0.3‰[35]. At TR163-25 the late Holocene (<3,500 years) is missing.

**Subsurface water oxygen concentrations.** To document upper-ocean oxygenation, we use the planktonic foraminifera I/Ca proxy from ref. [5]. The electrode potential of the iodate/iodide couple is very similar to that of denitrification[9]. In the surface ocean, iodide exists in well-oxygenated settings, which has been attributed to disequilibrium caused by biological activity and photochemical reduction of iodate to iodide[36–38]. The oxidation of iodide back to iodate is slow and may take from months to up to 40 years[20].

I/Ca ratios were measured on several planktonic foraminifera species covering a range of depth habits. Spinose species *Globigerinoides sacculifer* (ODP sites 849 and 1242) and *G. ruber* (ODP site 1242) typically live in the surface mixed layer, whereas non-spinose species *Pulleniatina obliquiloculata* (ODP site 849), *Globorotalia menardii* (ODP site 1242) and *Neogloboquadrina dutertrei* (ODP sites 849 and 1242) live deeper, at or below the thermocline[39–41]. These depth habitat differences are expressed in the oxygen isotope records, with consistently depleted values for the warmer surface-mixed-layer species, and heavier values for the deeper- and cooler-water-dwelling species (Fig. 2). Pristine planktonic foraminifera were rigorously cleaned using a previously published method[42] before I/Ca analyses.

It is unlikely that lower deglacial I/Ca ratios at ODP site 849 are due to productivity changes; modern open ocean productivity pulses do not lower $IO_3^-$ to concentrations below 0.25 μM in oxygenated water, suggesting that our planktonic foraminifera I/Ca signals are most likely driven by the oxygen concentration of subsurface water and not by productivity[5].

**Nitrogen isotopes.** Bulk sedimentary $\delta^{15}N$ can indirectly reflect the extent of suboxia within the upper water column, near the core site, owing to the enrichment of $^{15}N$ in residual nitrate during denitrification[43]. Nitrogen isotopes can, however, also be affected by other processes such as dilution of the isotopic signal given the fraction of nitrate consumed by denitrification in suboxic zones[44], the input of nitrate by advection from distant suboxic zones[16], the addition of low $^{15}N$ nitrogen by $N_2$ fixation, and partial nitrate uptake by phytoplankton at remote locations[18,45], and so are not unambiguous recorders of the local extent of suboxia.

Bulk sedimentary $\delta^{15}N$ at both ODP site 1242 and TR163-25 (Extended Data Fig. 2) show lower values during the LGM, consistent with other $\delta^{15}N$ records within the region[18]. Only at ODP site 1242 are sufficiently low oxygen concentrations ($[O_2] < 2–4$ μmol $kg^{-1}$) found for denitrification to occur today[46], and only at depths of more than 300 m in the water column (Fig. 1). This is below the depth from which wind-driven upwelling draws. Thus, the nitrogen incorporated in organic matter at the surface and exported to depth, producing the bulk sedimentary $\delta^{15}N$ record, does not directly reflect local suboxia at either site. Instead, the records at these locations are likely to reflect regional changes in nitrogen cycling, as is true for the similar records found throughout the ETP[18]. These changes could have included lower rates of denitrification despite similar volumes of OMZ waters, or more complete nitrate consumption during denitrification leading to a weaker isotopic signal.

Notably, nitrogen isotope values at the Gulf of Tehuantepec, where the most active water column denitrification occurs today, were similar during the LGM and the late Holocene (7‰), consistent with similarly active denitrification during both times[17].

**Changes in the soft tissue pump.** The $\delta^{13}C$ value of dissolved inorganic carbon ($\delta^{13}C_{DIC}$) depends on both the preformed component ($\delta^{13}C_{pre}$) and soft tissue components ($\delta^{13}C_{soft}$). The latter term results from the remineralization of organic matter and is related through stoichiometric ratios to oxygen consumption and carbon storage. The $\delta^{13}C_{pre}$ is determined by temperature, salinity, $p_{CO_2}$, alkalinity, the whole ocean average $\delta^{13}C$, and the disequilibrium of surface waters when they sink. Often overlooked, the $\delta^{13}C_{pre}$ value is sensitive to changes in the soft tissue pump and ocean circulation in addition to globally averaged $^{13}C/^{12}C$.

If we ignore the small impact of the carbonate pump on carbon isotopes, the $\delta^{13}C_{DIC}$ at an arbitrary point in the ocean interior is given by:

$$\delta^{13}C_{DIC} = \frac{\delta^{13}C_{pre} \times DIC_{pre} + \delta^{13}C_{soft} \times DIC_{soft}}{DIC_{tot}}$$

The LGM–Holocene change (D) in all quantities is approximately:

$$D\delta^{13}C_{DIC(LGM-Hol)} = \frac{D(\delta^{13}C_{pre} \times DIC_{pre})}{DIC_{tot}} + \frac{D(\delta^{13}C_{soft} \times DIC_{soft})}{DIC_{tot}}$$

This equation includes a number of unknowns, which can be simplified using three assumptions. First, that changes in $\delta^{13}C_{soft}$ were negligible. Second, that although the shallow and deep sites certainly would have had different preformed components, the glacial–interglacial change in the preformed component, $D(\delta^{13}C_{pre} \times DIC_{pre})$, was the same at the two sites. Third, that the change in $DIC_{soft}/DIC_{tot}$ was small. This then gives the change in $\delta^{13}C_{pre}$ between the two depths in (z2–z1) as:

$$D\delta^{13}C_{DIC(z2-z1)} = \delta^{13}C_{soft} \times \frac{DDIC_{soft(z2-z1)}}{DIC_{tot}}$$

The $\delta^{13}C_{DIC}$ data show the relative change between the deep and shallow site, from 0.2‰ during recent times to −0.3‰ during the LGM, a change of 0.5‰. Assuming $\delta^{13}C_{soft}$ is −23‰ and DIC is about 2,200,

$$-0.5 = -23 \times \frac{DDIC_{soft}}{2{,}200} \quad \text{and} \quad DDIC_{soft} = 48$$

This would suggest a glacial–interglacial relative change in oxygen utilization between the two depths of $48 \times 140[O_2]/106\,C = 63$ μM. Our new reconstructions show that oxygen concentrations at the two depths converged at the LGM.

At present, oxygen concentrations at the deeper site are about 65 μM higher than at the shallow site, which would suggest that, on the basis of the $\delta^{13}C$, oxygen concentrations during the LGM should have been the same at the two sites. This is essentially what we observe, supporting the assumption of similar changes in the preformed components in the waters bathing the two depths. Note that this is not to say that the preformed components were constant. Rather, they both changed considerably, but in a coordinated way, owing to the whole ocean change of 0.34‰, and complex interconnected changes in temperature, alkalinity, salinity, $p_{CO_2}$ and air–sea exchange dynamics. Because those changes appear to have occurred together at these depths, we can then take the assumption that, for the Pacific at depths between approximately 1 km and 3 km, there was a uniform LGM–recent change in $\delta^{13}C_{pre}$. As a result, the relative changes in $\delta^{13}C$ between sites should have been dominated by changes in $DIC_{soft}$, enabling a large-scale budget to be constructed.

Between depths of 1.4 and 3 km, the average difference in $\delta^{13}C$ of DIC between the LGM and recent times is $-0.10‰ \pm 0.13‰$. At TR163-25, LGM–recent $\delta^{13}C$ was −0.30‰, whereas dissolved oxygen values were decreased by 65 μmol $kg^{-1}$ compared with recent times (Extended Data Fig. 3). Thus, with our new constraints, the average decrease of 0.10‰ in the LGM–recent $\delta^{13}C$ of DIC between 1.4 and 3 km in the Pacific can be translated to oxygen concentrations that were 22 μmol $kg^{-1}$ lower ($-0.10/0.30 \times 65$) than preindustrial (not accounting for changes in preformed oxygen disequilibrium). Assuming a 2.5 °C decrease in average deep Pacific temperature and a 1 unit increase in salinity (see ref. [47]), the saturated dissolved oxygen concentration (calculated using the equations in ref. [48]) would be 353 μmol $kg^{-1}$, nearly 20 μmol $kg^{-1}$ higher than at present. Apparent oxygen utilization (difference between saturation oxygen concentration and measured oxygen concentration) was therefore increased by 42 μmol $kg^{-1}$ during the LGM in the deep Pacific. Extrapolated across water depths between 1.4 and 3 km, this amounts to an increase in respired carbon of 90 Gt C. If similar conditions and changes in $\delta^{13}C_{pre}$ applied across the whole of the deep Pacific (all depths >1.4 km), a volume over which the average LGM–recent $\delta^{13}C$ is $-0.17‰ \pm 0.18‰$, then the corresponding increase in glacial respired carbon would amount to 200 Pg C.

## Data availability

Data generated during this study are available from https://doi.pangaea.de/10.1594/PANGAEA.891185.


31. Umling, N. E. & Thunell, R. C. Synchronous deglacial thermocline and deep-water ventilation in the eastern equatorial Pacific. *Nat. Commun.* **8**, 14203 (2017).
32. Blaauw, M. & Christen, J. A. Flexible paleoclimate age-depth models using an autoregressive gamma process. *Bayesian Anal.* **6**, 457–474 (2011).
33. Codispotti, L., Yoshinari, T. & Devol, A.H. in *Respiration in Aquatic Ecosystems* (eds del Giorgio, P. & Williams, P.) Ch. 12 (Oxford Univ. Press, Oxford, 2005).
34. Mix, A. C. et al. *Proc. ODP, Init. Rep.* https://doi.org/10.2973/odp.proc.ir.202.113.2003 (2003).
35. Eide, M., Olsen, A., Ninnemann, U. S. & Eldevik, T. A global estimate of the full oceanic $^{13}C$ Suess effect since the preindustrial. *Global Biogeochem. Cycles* **31**, 492–514 (2017).
36. Chance, R. et al. Seasonal and interannual variation of dissolved iodine speciation at a coastal Antarctic site. *Mar. Chem.* **118**, 171–181 (2010).
37. Spokes, L. J. & Liss, P. L. Photochemically induced redox reactions in seawater, II. Nitrogen and iodide. *Mar. Chem.* **54**, 1–10 (1996).
38. Chance, R., Baker, A. R., Carpenter, L. & Jickells, T. D. The distribution of iodide at the sea surface. *Environ. Sci. Process Impacts* **16**, 1841–1859 (2014).
39. Fairbanks, R. G., Sverdlove, M., Free, R., Wiebe, P. H. & Bé, A. W. H. Vertical distribution and isotopic fractionation of living planktonic foraminifera in the Panama Basin. *Nature* **298**, 841–844 (1982).
40. Ravelo, A. C. & Fairbanks, R. G. Oxygen isotopic composition of multiple species of planktonic foraminifera: recorders of modern photic zone temperature gradient. *Paleoceanography* **7**, 815–831 (1992).
41. Farmer, E. C., Kaplan, A., de Menocal, P. B. & Lynch-Stieglitz, J. Corroborating ecological depth preferences of planktonic foraminifera in the tropical Atlantic with the stable isotope ratios of core top specimens. *Paleoceanography* **22**, (2007).
42. Barker, S., Greaves, M. & Elderfield, H. A study of cleaning procedures used for foraminiferal Mg/Ca paleothermometry. *Geochem. Geophys. Geosyst.* **4**, 8407 (2003).
43. Altabet, M. A. et al. The nitrogen isotope biogeochemistry of sinking particles from the margin of the Eastern North Pacific. *Deep Sea Res. Part I* **46**, 655–679 (1999).
44. Deutsch, C., Sigman, D. M., Thunell, R. C., Meckler, A. N. & Haug, G. H. Isotopic constraints on glacial/interglacial changes in the oceanic nitrogen budget. *Global. Biogechem. Cycles* **4**, 1–22 (2004).
45. Farrell, J. W., Pedersen, T. F., Calvert, S. E. & Nielsen, B. Glacial–interglacial changes in nutrient utilization in the equatorial Pacific Ocean. *Nature* **377**, 514–517 (1995).
46. Devol, A. H. in *Nitrogen in the Marine Environment* 2nd edn (eds Capone, D. G. et al.) 263–301 (Academic, Burlington, 2008).
47. Adkins, J. F., McIntyre, K. & Schrag, D. P. The salinity, temperature, and $\delta^{18}O$ of the glacial deep ocean. *Science* **298**, 1769–1773 (2002).
48. Debelius, B., Gómez-Parra, A. & Forja, J. M. Oxygen solubility in evaporated seawater as a function of temperature and salinity. *Hydrobiologia* **632**, 157–165 (2009).
49. Robinson, R. S., Martinez, P., Pena, L. D. & Cacho, I. Nitrogen isotope evidence for deglacial changes in nutrient supply in the eastern equatorial Pacific. *Paleoceanography* **24**, PA4213 (2009).
50. Rafter, P. A. & Charles, C. D. Pleistocene equatorial Pacific dynamics inferred from the zonal asymmetry in sedimentary nitrogen isotopes. *Paleoceanography* **27**, PA3102 (2012).
51. Boyer, T. P. et al. *World Ocean Database 2013* (ed. Levitus, S.) (NOAA Atlas NESDIS 75, 2013).

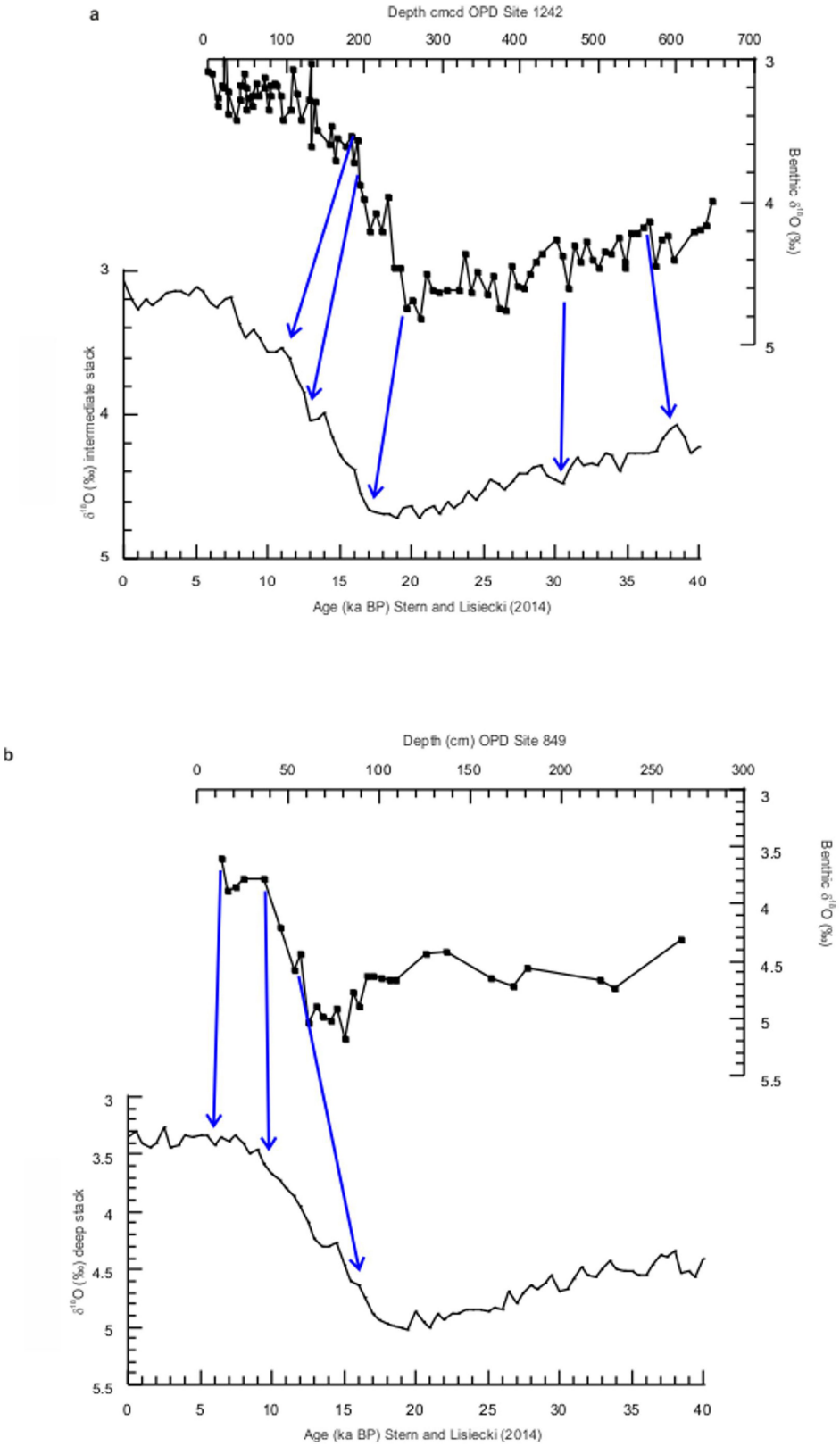


**Extended Data Fig. 1 | Details of age models for ODP sites 1242 and 849. a**, Matching the ODP site 1242 benthic composite $\delta^{18}O$ record to the Pacific Intermediate water stacked $\delta^{18}O$ record of ref. [29]. **b**, Matching the ODP site 849 benthic composite $\delta^{18}O$ record to the Pacific deep water stacked $\delta^{18}O$ record of ref. [29].

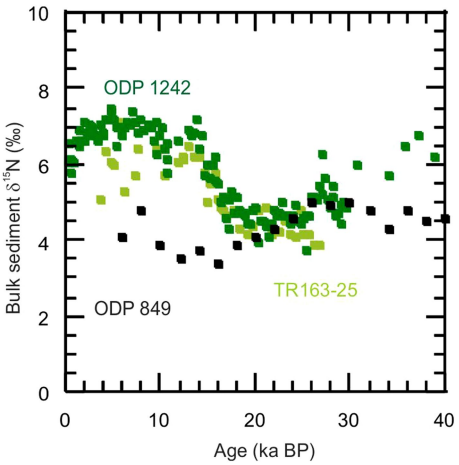


**Extended Data Fig. 2 | Regional bulk sedimentary $\delta^{15}N$ records.** Dark green, bulk sedimentary $\delta^{15}N$ record of ODP site 1242[49]; light green, bulk sedimentary $\delta^{15}N$ record of TR163-25 (this work); black, bulk sedimentary $\delta^{15}N$ record of ODP site 849[50].

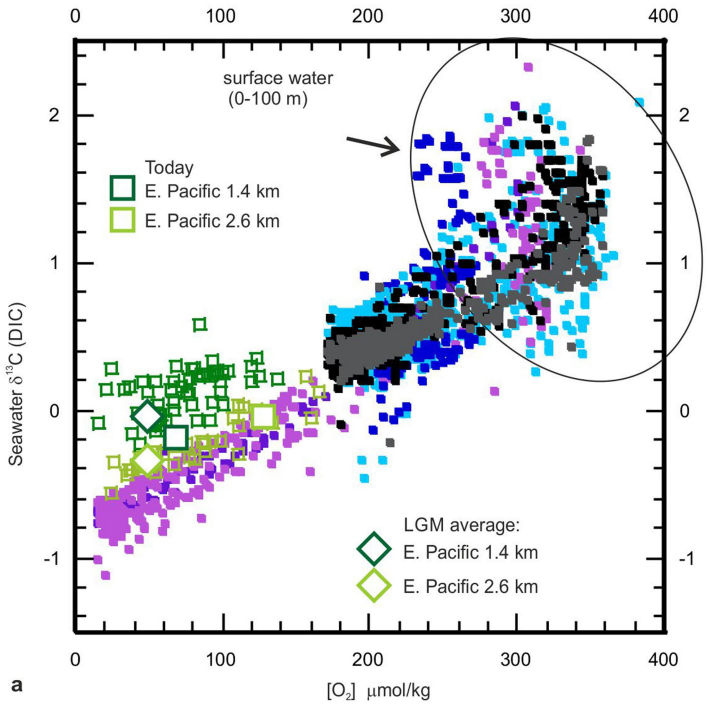


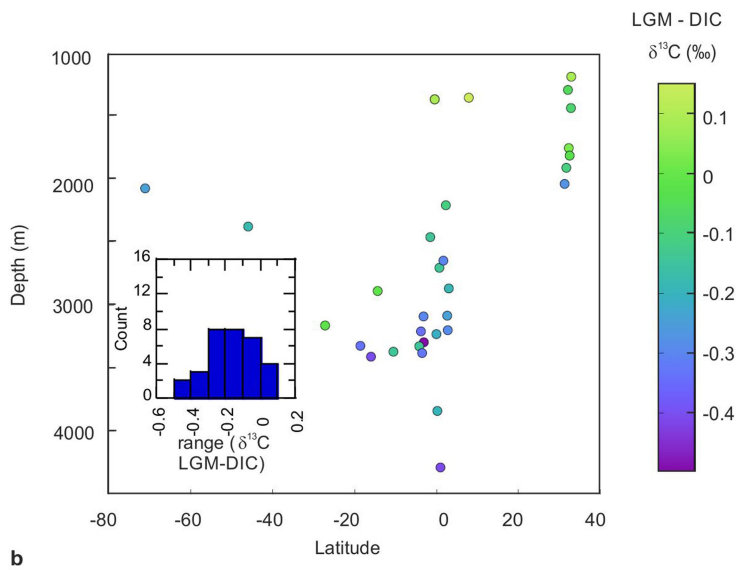


**Extended Data Fig. 3 | Overview and LGM evolution of carbon isotopes and oxygen concentrations in the eastern tropical Pacific. a**, Dissolved oxygen concentrations (modern: North Atlantic north of 50° N, dark blue; South Atlantic south of 50° S, light blue; southeast Pacific south of 50° S, black; southwest Pacific south of 50° S, grey; northeast Pacific north of 50° N, dark purple; northwest Pacific north of 50° N, light purple; and reconstructed for the past 40 kyr: ODP site 1242, dark green; TR163-25, light green) plotted against carbon isotopes of DIC of seawater (‰) (data from refs [28,51] using https://www.nodc.noaa.gov/OC5/SELECT/dbsearch/dbsearch.html. Square boxes represent modern values at the two sites; diamonds represent LGM values (average 18–22 kyr BP). **b**, Latitudinal profile of the difference in Pacific carbon isotopes between the LGM (18–22 kyr, from epifaunal benthic foraminifera) and recent (DIC) seawater carbon isotopes (extrapolated from ref. [34]). Inset, histogram of LGM-DIC $\delta^{13}C$ (waters deeper than 1.3 km) has a normal distribution (0.1‰ bin width).

**Extended Data Table 1 | Age control points for ODP sites 1242 and 849**

| Depth (cm) 1242 | Age (ka BP) 1242 | | Depth (cm) 849 | Age (ka BP) 849 |
|---|---|---|---|---|
| 0 | 0 | | 13 | 6 |
| 191 | 11 | | 37 | 10 |
| 196 | 13 | | 61 | 17.5 |
| 255 | 17 | | | |
| 461 | 30.5 | | | |
| 565 | 38 | | | |

Based on matching the benthic foraminiferal composite oxygen isotope records with the stacked records of ref. [29].

**Extended Data Table 2 | Age control points for TR163-25**

| TR163-25 depth (cm) | 14C age (14C years) | Error ±1σ | ΔR | Species |
|---|---|---|---|---|
| 40 | 7335 | 20 | 147±13 | *G. ruber* |
| 80 | 12895 | 45 | 1250±133 | *N. dutertrei* |
| 100 | 14250 | 60 | 1430±123 | *N. dutertrei* |
| 145 | 20850 | 130 | 2032±201 | *N. dutertrei* |

Based on $^{14}C$ dates and calculated reservoir ages.